Stability improvement of Au/Fe–La–Al$_2$O$_3$ catalyst via incorporating with a Fe$_x$O$_y$ layer in CO oxidation process

Caixia Qi*, Shudong Zhu, Huijuan Su, Hui Lin, Rengui Guan

School of Chemistry and Chemical Engineering, Yantai University, Shandong Applied Research Center of Gold Nanotechnology (Au-SDARC), Yantai 264005, PR China

ABSTRACT

Various amounts of α-Fe$_2$O$_3$ were incorporated into the parent Au/Fe–La–Al$_2$O$_3$ catalyst using post-adding iron nitrate precursor via the wetness impregnation method with water, ethanol, and acetone as solvents, respectively. Though post-addition of iron oxides makes gold particles aggregation with less catalyst activity than the parent one in the CO oxidation reaction, the most striking thing is that the Fe-modified catalysts present better online stability. At the same time, in situ thermal treatment can totally recover the activity of the spent Fe-modified catalysts but not the parent one. Water as a solvent performed better than ethanol and acetone; the corresponding catalysts exhibited the best catalytic performance with the most serious Au particle aggregation after post-addition of iron species.

© 2013 Elsevier B.V. All rights reserved.

1. Introduction

Supported Au catalysts for low-temperature oxidation of CO are becoming increasingly attractive in cleaning air, lowering automotive emissions and utilizing in protective gas masks, CO and CO$_2$ detectors [1,2]. Gold catalysts are superior to other noble metal catalysts, such as Pd and Pt, for great activity at ambient temperature and more tolerant to moisture than Hopcalite catalysts (a mixture of manganese and copper oxides) [3]. They can oxidize CO even at −77 °C in a wider range of concentration [4] and can be activated with moisture [5]. Few Au catalysts have been successfully applied in gas masks for CO removal via the CO oxidation reaction [6,7], including catalyst we developed [6], as well as in diesel emission control through partially replacing Pt and Pd [7]. The catalytic activity of our modified alumina supported Au catalyst for low-temperature CO oxidation was found stable for more than 7 years when properly stored in a desiccator [6,8]. However, hundreds of hours life of 0.2 g catalyst with 1.0 wt% Au loading, when performed in 1 vol% CO in air stream with a space velocity of 16000 ml h^{-1} g$_{cat}$$^{-1}$, is far beyond the industrial needs for a wider practical application, such as in an open system of tunnel.

In the recent years, more attentions have been given to gold catalysts for their stability and deactivation behavior [9–18]. Gold catalysts could be deactivated either in use or in storage due to

several reasons, such as particle size agglomeration [9–11,16], formation of carbonate-like species [5,12–17] and removal of hydroxyl groups from active sites [17] in CO oxidation and other morphological changes in gold clusters [18], and reduction of the support surface [19].

Although the nature of active sites for CO oxidation on supported Au catalysts is still being elucidated [20–23], many researchers agree that the interaction between Au particles and the supporting oxide at their contact perimeter plays an important role in determining the catalytic activity of the Au nanoparticles [20,24–26]. To date, there is however no clear explanation regarding the contribution of Au-oxide contact perimeter on the stability of Au catalysts. There are two approaches for increasing Au-oxide contact area in the Au catalyst. The first one is to reduce the size of the Au nanoparticles, as demonstrated in many supported Au catalysts. The second approach is to reduce the particle size of support, as demonstrated by Zhang et al. [27]. The latter catalyst shows excellent activity and on-line stability for the CO oxidation in dry air.

In contrast to supported Au catalysts (Au on oxide), Bollinger and Vannice found that deposition of TiO$_x$ overlayers onto inactive Au powders can produce very active TiO$_2$–Au catalyst for CO oxidation [28]. Rodriguez et al. reported that CeO$_x$ and TiO$_x$ nanoparticles grown on Au (1 1 1) are very active in water gas shift reaction [29]. In addition, an active CO oxidation catalyst was obtained through insertion of Au nanoparticles in the channel of MCM-48 [30]. A high temperature stable catalyst was reported by confining nanogold in ZrO$_2$ shell [31]. It can be expected, therefore, that post-deposition of proper oxides or other materials to form a kind of

* Corresponding author. Tel.: +86 535 6902233; fax: +86 535 6902233.
E-mail address: qicx@ytu.edu.cn (C. Qi).

sandwich-type (oxide-Au-oxide, or supported Au catalysts with porous cover) catalyst could be an alternative to increase Au-support interaction through creating more Au-support contact perimeters. Tanaka et al. [32,33] and Shou et al. [34] once observed that Pt/TiO$_2$, Pt/Al$_2$O$_3$ and Au/TiO$_2$ were significantly activated via deposition of a large quantity of FeO$_x$ for the selective CO oxidation in presence of H$_2$ or H$_2$O or both. The particle size of active metal was large because the impregnation method was applied to deposit Pt or Au on the support of TiO$_2$ or Al$_2$O$_3$. In addition, iron oxide has been demonstrated in many researches as an active support for Au catalysts in the CO oxidation [4,35–40]. The inclusion of FeO$_x$ reveals a beneficial effect on the stability of the catalysts with TiO$_2$, SnO$_2$, and CeO$_2$ used as supports [19]. Larger activity in CO oxidation was recently reported over a dispersed Au@Fe$_2$O$_3$ core–shell structured catalyst than an Au/Fe$_2$O$_3$ catalyst prepared via colloidal deposition [41].

In this work, an attempt was made to create new active sites for improvement of the relevant stability and to filter or convert or prevent the catalyst from attacks by exterior unknown harmful molecules and dusts in air. We deposited iron oxide on a Fe and La modified alumina supported Au catalyst, which we found very active for low temperature CO oxidation [42], via the simplest method, i.e. incipient wetness impregnation. Water, ethanol, or acetone was used as a solvent, respectively. Improvement in the online stability of the corresponding modified catalysts for the CO oxidation process was observed. The decrease in activity of the catalyst can be avoided through optimizing the preparation parameters.

2. Experimental

2.1. Catalyst preparation

2.1.1. Preparation of parent Au catalyst

Firstly, Fe, La modified γ-Al$_2$O$_3$ composites with 1:1 atomic ratio of Fe:La was prepared via the incipient wetness impregnation method. A given amount of γ-Al$_2$O$_3$ beads (Shandong Alumina Company, China) with mean diameter of ca. 0.8–1.5 mm was added to a solution of iron nitrate and lanthanum nitrate under stirring. The mixture was stirred for 12 h, followed by drying at 80 °C for several hours and the calcination was performed at 750 °C for 4 h. The resultant Fe and La modified Al$_2$O$_3$ support, with possible formation of a small amount of LaFeO$_3$ on the surface of γ-Al$_2$O$_3$ [42] was named as FLA.

Subsequently, the parent Au/FLA catalyst was prepared through a modified deposition–precipitation method [8,10]. A certain amount of FLA support was added to a solution of HAuCl$_4$·xH$_2$O (Sinopharm Chemical Reagent Company, Shanghai, China) with a pH of 9.0 that was adjusted with 1.0 M KOH solution. Then, 50 ml of aqueous ammonia solution with a pH of 11 was added after few hours. Extensive washing with de-ionized water was then followed until it became free of chloride ions, detected with an aqueous solution of AgNO$_3$. The resulting catalyst precursor was dried at 60 °C overnight and then reduced in flowing hydrogen atmosphere at 300 °C for 2 h.

2.1.2. Post-deposition of iron oxide on the parent catalyst

Fe(NO$_3$)$_3$·9H$_2$O with 1, 5, 10, 15, or 20 wt% of theoretical Fe content was loaded to the parent Au catalyst via the incipient wetness impregnation method, while water, ethanol or acetone was used as a solvent, respectively. The mixture was dried at 80 °C and then calcined at 350 °C for 2 h.

The Au loading in parent Au/FLA catalyst was measured as 1.36 wt%. The inductively coupled plasma (ICP) analysis suggested that none of gold leached off the parent catalyst in the process of post-addition of the iron species. An amount of 8.54, 8.47 or

8.38 wt% Fe was added to the parent catalyst with respect to 10 wt% Fe/Au/FLA catalysts using water, ethanol or acetone as a solvent. These three solvents did not make any obvious difference on the actual amount of post-added Fe.

2.2. Catalytic activity of CO oxidation

The CO oxidation process was examined in a continuous flow fixed-bed reactor under atmospheric pressure. The reaction feed was passed through the catalytic bed with a space velocity of 16,000 ml h^{-1} g$_{cat}$$^{-1}$. Unless otherwise indicated, 200 mg of catalyst was used as prepared without any additional treatment. The reactor effluent was online analyzed with a gas chromatograph (Haixin GC-950, Haixin Chromatographic Instruments Company, Shanghai, China) equipped with a thermal conductivity detector and a 5 Å molecular sieve column.

2.3. Catalyst characterization

The crystal structure of added iron compound in final Au catalyst was characterized with powder X-ray diffraction (XRD) technique on a powder diffractometer (Shimadzu XRD 26100, Shimadzu Scientific Instruments Company, Kyoto, Japan) using Cu Kα radiation (0.15405 nm) source at a voltage of 40 kV and a current of 30 mA. The catalyst beads were crushed and placed in a quartz holder and then scanned over the range 2θ from 10 to 70° at a rate of 5.0° min^{-1}. Diffraction peaks of crystalline phases were compared with those of standard compounds reported in the JCPDS data file.

The gold and iron contents of prepared catalysts were measured using atomic adsorption spectroscopy technique (Shimadzu AA-2670, Shimadzu Scientific Instruments Company, Kyoto, Japan). Accurately weighted sample was dissolved into aqua regia at 60 °C and diluted with deionized water to 50 ml or 100 ml and analyzed along with known solutions prepared with Au and Fe standards.

The gold particle size and size distribution in Au catalysts were measured with high resolution transmission electron microscopy technique (HRTEM) (JEOL JEM-2100, JEOL Company, Tokyo, Japan) operating at 200 kV. A small amount of sample powder was put into the sample tube filled with 95% ethanol solution. After agitation under supersonic environment for several minutes, one drop of the dispersed slurry was dispersed onto a carbon coated copper mesh and dried under light at room temperature.

The location and distribution of post-added iron compound in the final catalysts were examined using scanning electron microscopy technique (Hitachi S-3500N SEM, Hitachi Company, Tokyo, Japan) operating at 25 KeV. An equipped energy dispersive X-ray (EDX) spectroscopy technique (Oxford Inca, Oxford Instruments Analytical Company, UK) was carried out for line scan and elemental mapping. The catalyst was buried with a resin and then polished and coated with gold before examination.

The room temperature organic (RTO) sampling [43] and TEM technique equipped with EDX were further performed to confirm the deposition locations of post-added Fe species in Fe-modified Au/FLA catalysts. The catalyst beads were carefully crushed and then few-micrometer pieces with certain thickness from outmost layer were chosen and placed on the polished metal slices. These pieces were then buried without disturbing by any metal, such as copper, in an organic solution with pH of 8 at room temperature via electron deposition of metal complex. The metal slice with buried particles was then polished from two opposite faces until the buried catalyst pieces were exposed. Finally, these micrometer large catalyst pieces were cut into nanometer thickness section using argon-ion cutting apparatus and were made ready for electron microscopy observations. The EDX elemental mapping was
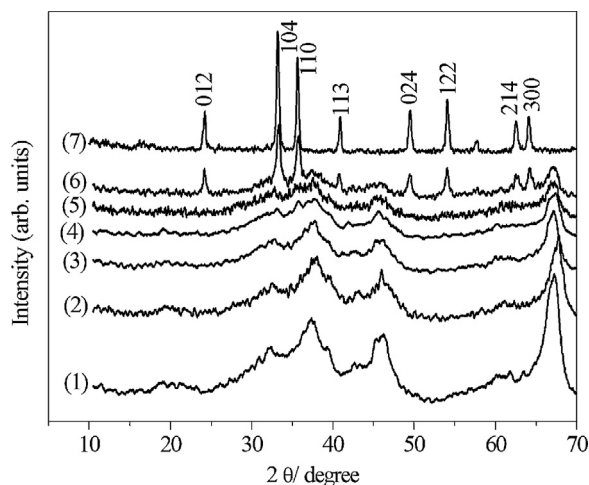
Fig. 1. XRD patterns of (1) Al_2O_3, and Fe-modified Au/FLA catalysts prepared with water as a solvent containing: (2) 1.0, (3) 5.0, (4) 10, (5) 15, (6) 20 wt% of Fe, and (7) α-Fe_2O_3.

Fig. 2. XPS spectra of Fe in 10 wt% Fe/Au/FLA catalyst with water as a solvent.

used to measure the distribution of elements in the piece of catalyst.

The nitrogen adsorption and desorption isotherms were measured at 196 °C using a Micromeritics ASAP 2010 pore size and adsorption analyzer system (Micromeritics Company, Norcross, GA, USA). Surface areas, pore volumes, and pore sizes were determined using nitrogen desorption data in the relative pressure in the range of 0.01–0.35 using the BET equation. Samples were degassed at 120 °C for 5 h under vacuum before N_2 adsorption measurements.

3. Results

3.1. Crystal structure of the post-added Fe species

Fig. 1 shows the XRD patterns of Fe_xO_y/Au/FLA (FLA stands for Fe–La–Al_2O_3) with various post-added iron content when water was used as a solvent. The patterns reveal that the intensities of the characteristic peaks of Al_2O_3 at 67.3°, 37.3°, and 45.7° decrease with an increase in the amount of posted-added iron. Whereas new peaks at 24.2°, 33.2°, 35.6°, 40.9°, 49.7°, 54.1°, 62.5°, and 54.1° clearly appear with respect to 20 wt% posted-added iron, in conformity with crystal planes of (0 1 2), (1 0 4), (1 1 0), (1 1 3), (0 2 4), (1 2 2), (2 1 4), and (3 0 0), respectively, for α-Fe_2O_3 (JCPDS 33-0664). Two strongest peaks with (1 0 4) and (1 1 0) planes can be recognized with very low intensity for samples with 15 and 10 wt% post-added Fe, meaning much less crystal of α-Fe_2O_3 existed in this two samples. None of the new peaks was observed for other samples with less post-added Fe species. In addition, none of the distinct gold peaks at 2θ of 38.2°, 44.5°, and 64.5° is apparently visible, indicating highly dispersion of nanogold particles in the catalyst and Au loading less than the detection limitation. Similar results were observed when ethanol or acetone was used as the solvent (data not presented in this paper).

The chemical state of Fe in the above catalyst was further investigated using an X-ray photoelectron spectroscopy technique. As shown in Fig. 2, the core level spectra of Fe 2p were curve fitted and four peaks for Fe 2p were observed in the spectra. Peaks corresponding to 710.6 and 723.8 eV are ascribed to +3 states of iron. The energy difference between Fe 2p 3/2 and Fe 2p 1/2 levels is 13.2 eV, which is characteristics of Fe^{3+} state [44], whereas 708.1 and 722.1 eV are attributed to +2 oxidation states [45]. This observation suggests that some of Fe (II) is presented in the catalysts of 10 wt%Fe/Au/FLA.
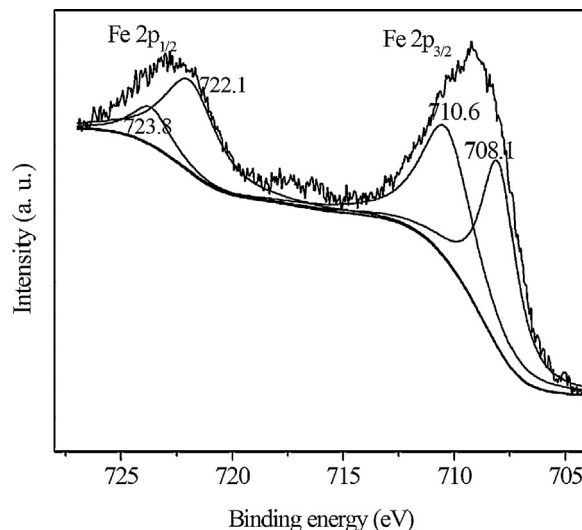
3.2. Location and distribution of post-added Fe oxides

To examine the distribution of post-added Fe oxides, the section areas of few beads containing 10 wt% Fe/Au/FLA catalyst prepared with water as a solvent were observed using SEM-EDX technique. One of the corresponding elemental maps of Fe, La, and Al and their line-scan spectrum are shown in Fig. 3a and b, respectively. The La and Al atoms are homogenously dispersed in the section area of the catalyst bead whereas Fe atoms are concentrated on the edge of the catalyst bead, as indicated by a white circle in Fig. 3a and by stronger peaks in two sides of line-scan spectrum of Fe element in Fig. 3b. This indicates that most of the Fe species are located at the outermost layer of the catalyst. Similar results were observed when ethanol and acetone were used as solvent (data not shown here).

We carried out EDX measurements in conjunction with TEM examination for the outermost piece of 10 wt% Fe/Au/FLA catalyst bead with water as a solvent. Fig. 4a shows the related TEM micrograph. Along the white arrow, the color of the catalyst piece changes from bright to dark and the texture varies from loose to compact, being totally different from the end of the arrow. The elemental maps of Al, Fe, and Au elements in the same piece of sample are displayed in Fig. 4b. While Al and Au elements mainly reside in the central region, Fe elements are extensively present in the outer region, as well as few in the core region. Accordingly, we deduce that the post-added iron oxide forms an outer shell that covers the parent catalyst of Au/FLA, in consistence with the results from SEM-EDX examinations. The thickness of Fe oxide layer could be estimated as smaller than 150 nm. In addition, Au nanoparticles are homogeneously dispersed in the region except for out-layer iron oxide. This is clearly visible in EDX maps and TEM images, indicated by some black cycles. The inset of HRTEM image suggests that most of nanogold particles are smaller than 10 nm (Fig. 4).

On the other hand, a certain fraction of post-added iron oxides reasonably penetrates into the subsurface of the catalyst, which is supported by our N_2 adsorption–desorption experimental results. The N_2 adsorption–desorption isotherms for Fe-modified Au catalysts in Fig. 5(1) and (2) demonstrate that all belong to the Type IV isotherm. In comparison with the pore size distribution of the parent Au/FLA catalyst, small amount of post-added Fe (e.g., 1 wt% Fe) does not make apparent change. On the other hand, the pore size distributions move toward smaller pores for the three 10% Fe-modified catalysts with three kinds of solvents. This observation suggests that certain amounts of Fe-species are located in the larger pores of the parent catalyst, making the pores smaller than
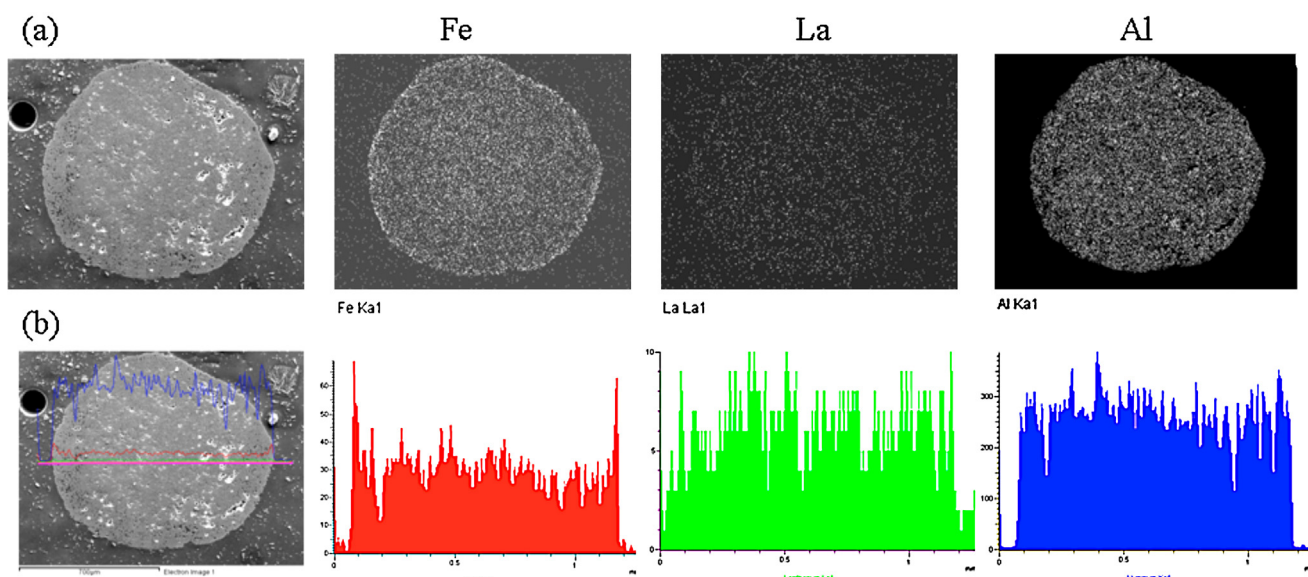
Fig. 3. (a) Elemental maps and (b) line scan spectrums of SEM-EDX analysis for the section area of the catalyst beads of 10 wt% Fe/Au/FLA prepared with water as a solvent.
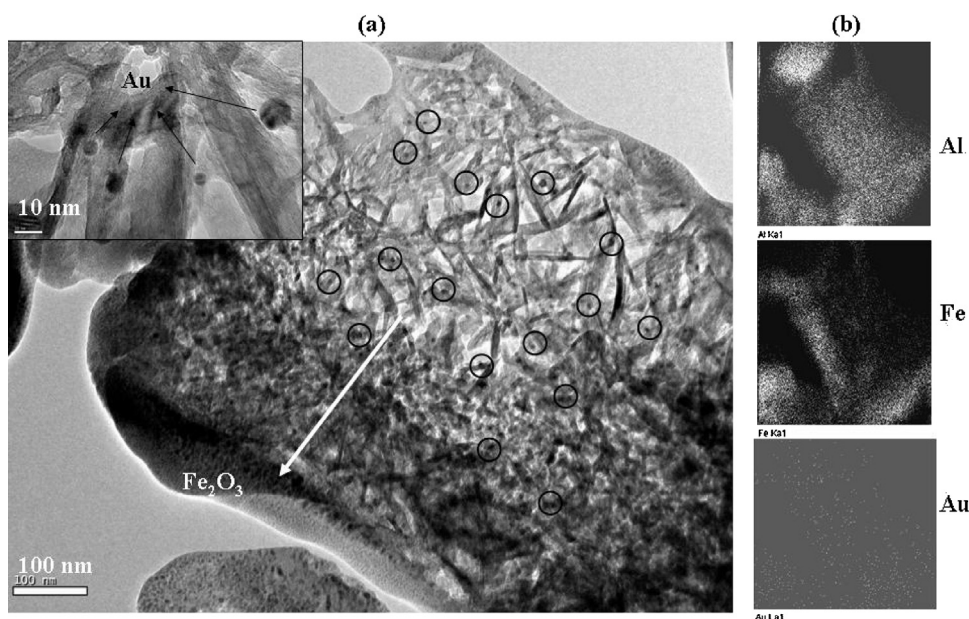

Fig. 4. (a) TEM images and (b) the EDX elemental maps of Fe, Al, and Au for one slice of outermost layer of the catalyst bead for 10 wt% Fe/Au/FLA prepared with water as a solvent.

before. The corresponding BJH surface areas, pores volumes, and mean pores diameters are compiled in Table 1. When water was used as a solvent, the surface areas and pore volumes decrease with increasing of post-added Fe amount; indicating the penetration of Fe-species into the subsurface of the parent catalyst. The increase in

surface areas for the other two modified catalysts with ethanol and acetone as the solvents than that of water could be a consequence of smaller pores in the newly formed Fe species. Some new contact interfaces between iron oxides and Au nanoparticles located on the surface and subsurface of the FLA support are thus formed to some extent.

3.3. Distribution of Au nanoparticles before and after post-addition of Fe species

Figure 6 displays a representative TEM micrograph and the size distribution of fresh Au/FLA catalyst. It reveals that Au nanoparticles are very small and uniformly dispersed in the sample with a mean diameter of 1.59 nm. As indicated in the inset of high-resolution TEM image in Fig. 4, for the Fe-modified catalysts, most of Au nanoparticles are randomly dispersed inside of FLA substrate
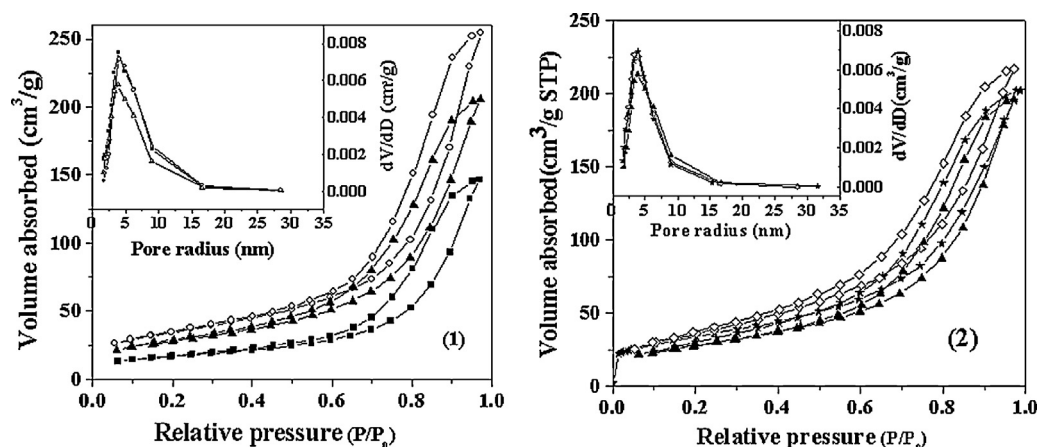
Table 1
BJH surface areas, pore volumes and mean pore radiuses of Fe-modified Au catalysts. The solvent used in the process is presented in the parentheses.

Catalysts	Surface area (m²/g)	Pore volume (cm³/g)	Pore radius (nm)
Au/FLA	167.9	0.42	3.93
1%Fe/Au/FLA	152.2	0.40	3.92
10%Fe/Au/FLA (water)	131.0	0.32	3.95
10%Fe/Au/FLA (ethanol)	158.5	0.34	3.92
10%Fe/Au/FLA (acetone)	148.2	0.33	3.91

Fig. 5. The N_2 adsorption–desorption isotherms and pore size distributions of (1) Fe/Au/FLA catalyst containing 0 (■), 1 (○) and 10 (▲) wt%; (2) 10 wt% Fe/Au/FLA prepared with water (▲), ethanol (◇), and acetone (★) as a solvent.

and the population decreases gradually from the edge to the center of the catalyst beads. However, the process of post-addition of Fe leads to nanogold particles aggregation with a wider distribution, as shown in Fig. 7. When water, ethanol, and acetone were used as the solvent, the mean diameters of gold particles increased to 4.0, 3.2, and 2.4 nm, respectively. It seems that the solvents exert certain influence on the gold particles aggregation with a sequence of acetone < ethanol < water.

3.4. Catalytic activity of Fe/Au/FLA catalysts

The activity of Fe/Au/FLA for CO oxidation decreased when the amount of the post-added Fe was increased whatever the solvent was used. As shown in Fig. 8, 1.0 vol % CO can be totally converted into CO_2 even at temperature as low as −23 °C over 0.2 g of the parent Au/FLA catalyst. The specific rate of CO conversion at 0 °C was measured in 30 min when small mass of the catalyst was applied and calculated as 7.69 mol g_{COAu}^{-1} h^{-1}. This result is comparable to the most active Au/oxide catalysts reported in the literatures [17,46–52]. For the Fe-modified catalyst with water as a solvent, the lowest temperature for 100% conversion of CO (LTCC) increased to 70 °C when 10 wt% Fe was added. In addition, the solvent used in the process of post-addition of Fe affected the activity of the Fe-modified catalyst. The LTCC for the three 10% Fe/Au/FLA catalysts has an upward sequence of water < ethanol < acetone, as shown in Fig. 9, opposite to the change in Au particle size in the

corresponding catalysts, as presented earlier in Section 3.3. That is to say, water as a solvent in the process of the post-addition of Fe onto the parent catalyst performs better than ethanol and acetone, although it makes more serious Au particles aggregation than the other solvents.

3.5. Online stability with time on the stream of 1.0 vol % CO in dry air

To compare the online stability with time on reactant stream for the parent catalyst of Au/FLA and the Fe-modified catalysts of Fe/Au/FLA, two temperatures of 0 and 80 °C over small mass of catalysts were applied respectively to ensure the conversion of CO below 100% and easy handing the reaction, because the modified catalysts are less active than the parent one. As shown in Fig. 10, the parent catalyst of Au/FLA losses its initial activity more dramatically than the three 10 wt% Fe/Au/FLA catalysts in the initial 10 h reaction, indicating less online stability. With an increase in post-added iron amount, online stability of the modified catalysts enhanced. In addition, the data in Fig. 10 also suggests the different influences in online stability of Au catalysts are caused by three types of solvents. Basically, water as a solvent performs better than ethanol and acetone.

The catalyst was then in situ activated at 300 °C for 1 h when the conversion of CO decreased to approximately 20%, the activity of parent Au/FLA catalyst diminished, whereas the total activity on
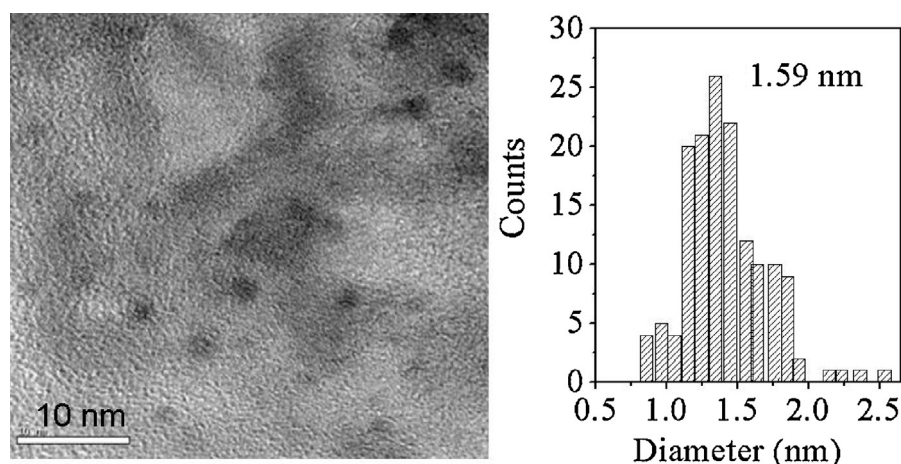

Fig. 6. TEM image of the parent Au/FLA catalyst and size distribution of Au particles. The number indicates the mean diameter of gold particles.
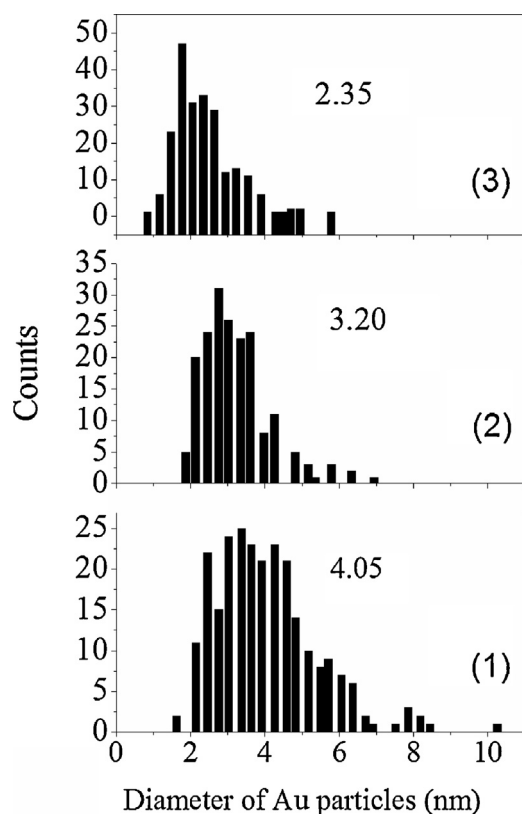
Fig. 7. Size distribution of Au particles in fresh catalysts of 10 wt% Fe/Au/FLA with (1) water, (2) ethanol or, (3) acetone as a solvent, respectively. The numbers indicate the mean diameters of gold particles.

recoveres of the three Fe-modified catalysts were observed simultaneously with an improvement in online stability. Basically, the Fe-modified catalyst with water as a solvent presents the best performance, both in activity on recovery and in online stability. Treatment for 1 h at 300 °C can enhance the conversion of CO from 60% to 100% and maintain it for more than 20 h. This indicates that the post-added Fe oxides in the outer catalyst layer somehow play a role in protection, as we expected in preventing the catalyst from quick deactivation.

3.6. Further enhancement in activity and online stability of Fe/Au/FLA

Fig. 6 clearly demonstrates that the process of post-addition of Fe species results in considerable growth of gold nanoparticles,
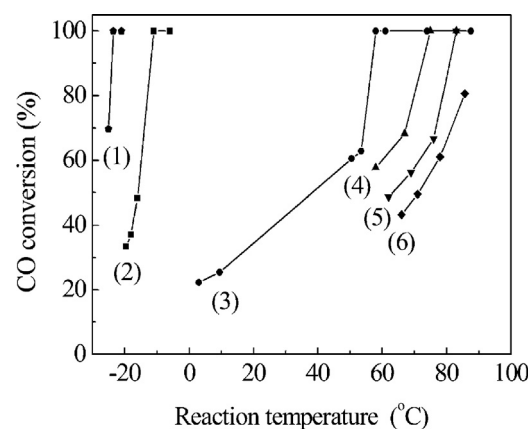

Fig. 8. CO oxidation over the catalysts of (1) the parent Au/FLA catalyst, and Fe/Au/FLA containing: (2) 1, (3) 5, (4) 10, (5) 15, and (6) 20 wt% post-added Fe nominally (water was used as a solvent; feed = 1.01 vol % CO in air; flowrate = 100 ml min^{-1}).

especially when water was used as the solvent. Although it is difficult to exclude the possibility that the blockage of active sites by post-added metals oxides leads to decrease in activity, we assume that the least activity of the Fe-modified catalyst of 10% Fe/Au/FLA is partially due to the larger gold particles because the activity of supported gold catalysts strongly depends on the particle size [21,24,53–56]. The preparation procedure was therefore modified through carrying out one-step reduction after adding Fe species. The size of gold particle was thus relatively reduced and the catalytic activity for the CO oxidation was therefore greatly enhanced, as shown in Fig. 11A. 0.2 g sample of the newly prepared 10% Fe/Au/FLA catalyst (prepared with water) could completely convert 1.0 vol % CO at a temperature as low as to 30 °C, 40 °C lower than the previous one. The initial rates of CO conversion at 25 and 80 °C are 0.48 and 2.6 mol$_{CO}$ g$_{Au}$$^{-1}$ h^{-1}, almost 4–5 times greater than the rates of 0.091 and 0.67 mol$_{CO}$ g$_{Au}$$^{-1}$ h^{-1} on the previous catalyst at identical reaction temperatures.

For a comparable activity comparison, the newly prepared 10% Fe/Au/FLA catalyst was tested at 80 °C for longer than 20 h in dry and wet streams of 1 vol % CO in air. About 3.01 vol % of water vapor was introduced via passing the feed stream through a water saturator at 30 °C when the catalyst was tested in wet air. In comparison with the parent Au/FLA catalyst, the online stabilities with time on dry and wet streams were also enhanced, as shown in Fig. 12. This observation indicates that an acceptable activity and improved online stability can be achieved over an Au catalyst covered with a layer of iron oxides.
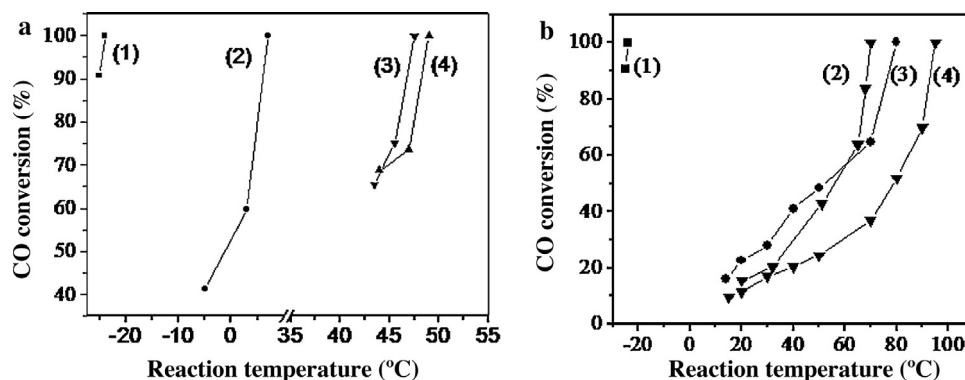

Fig. 9. CO oxidation on (1) the parent Au/FLA catalyst and Fe/Au/FLA prepared with (2) water, (3) ethanol or (4) acetone as a solvent, respectively. The nominal post-added Fe amounts were (a) 1.0 and (b) 10 wt%.
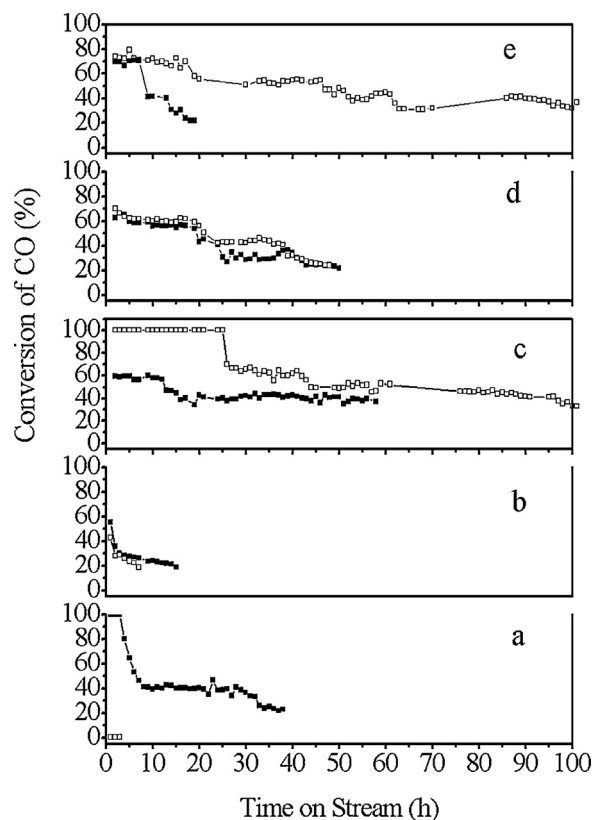
Fig. 10. CO conversion as a function of reaction time on reactant stream over the Au catalysts of (a) the parent Au/FLA catalyst, (b) 1.0 wt% Fe/Au–FLA (water was used as a solvent), 10 wt% Fe/Au–FLA with (c) water, (d) ethanol or, (e) acetone as a solvent, respectively. The reaction temperatures were 0 °C for (a) and (b) catalysts, and 80 °C for others. Solid symbols are for first runs, open symbols are for after in situ thermal treatment.
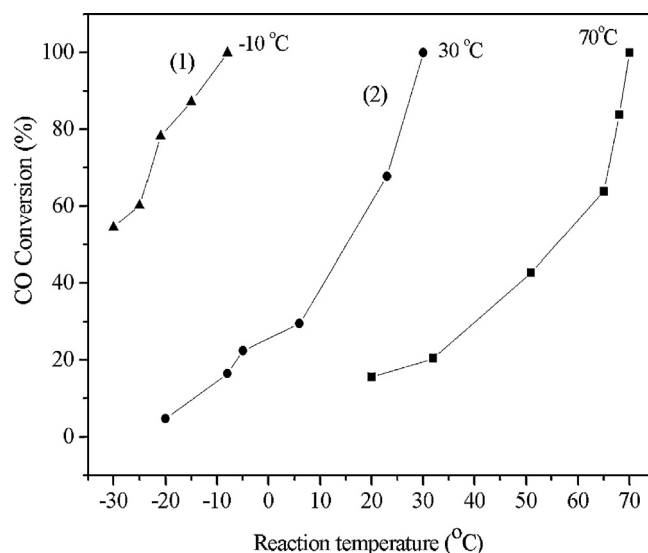

Fig. 11. Light curve of CO oxidation over (1) parent Au/FLA catalyst, (2) newly, and (3) previously prepared 10 wt% Fe/Au/FLA prepared with water as a solvent.

4. Discussion

The results presented in this paper indicate that the incorporation of an iron oxides layer can improve online stability of the Au/Fe–La–Al$_2$O$_3$ catalyst in the CO oxidation reaction. Moreau and Bond [19] once reported that the addition of a small amount of iron provided beneficial effect on the stability of Au catalysts with TiO$_2$, SnO$_2$, and CeO$_2$ as the principle supports. Improved stability and activity is ascribed to gold particles being in contact with an iron phase as FeO(OH). It should be mentioned that their catalysts were only dried at room temperature. The iron component remained as the hydroxide or the hydrated oxide and calcination removed the stabilization effect. In our study, the Fe-modified catalysts were calcined at 350 °C after post-addition of iron nitrate on the reduced Au/FLA catalyst. The iron component is mainly
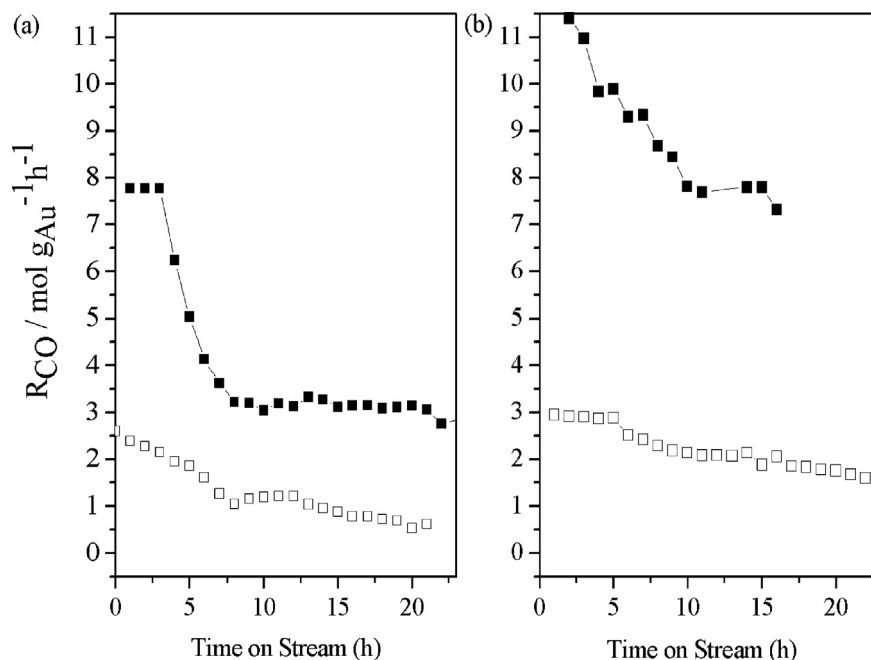

Fig. 12. CO conversion in (1) dry and (2) wet air as a function of reaction time on streams (a) at 0 °C over the parent Au/FLA catalyst (solid symbols) and (b) at 80 °C over newly prepared 10 wt% Fe/Au–FLA catalyst with water as a solvent (open symbols).

composed of α-Fe_2O_3. However, small amounts of FeO(OH) entities could exist. The better activity and stability of Fe-modified catalysts with water rather than acetone or ethanol as a solvent (see Figs. 9 and 10) are seemly in consistent with the deduction.

Recently, Haruta elucidated the interactions or relationships between five active states of gold (gold clusters, oxidic gold, bilayer Au atoms, gold nanoparticles, sponge and tube) and four factors (type of supports, size of Au species, −OH anion in the support and the content of moisture in gas-phase) in making gold catalytically active for low-temperature CO oxidation process [57]. The study comprehensively reflected the complexity of Au catalysis for such a simple catalytic reaction.

For a supported nanogold catalyst prepared through wet chemistry, the catalytic reactivity depends on the quantities of above mentioned types of active Au (except for sponge and tube) and hydroxyl groups, either on the support or close to gold particles, as well as kinds of support. Any moderate changes in the above matters may affect the online stability of a catalyst with time on reactive stream. The reduction of cationic Au and dehydration of ferrihydrite during reaction deactivates the catalyst [39]. A catalyst containing an optimum ratio of Au^{3+}/Au^0 calcined at a proper temperature has been suggested for practical application [37,38], although uncalcined Au/Fe_2O_3 catalyst enriched with Au^{3+} and FeO—OH entities, was found more active than calcined ones [36–39]. The same observation was also made by Wang et al. on an $Au/FeO_x/Al_2O_3$ catalyst [58].

In addition, Daniells et al. [59] studied CO oxidation over uncalcined and fresh Au on ferrihydrite support via few techniques. The authors proposed a mechanism that involves a carbonate/bicarbonate intermediate and observed enhancement of the rate with the presence of surface OH. The activity of the sample seems to be a function of the presence of −OH species, the rate of desorption of CO_2, or decomposition of surface carbonates. It appears that the amount of −OH species in a catalyst largely determines the activity of an Au catalyst for low temperature CO oxidation. The involvement of −OH species, directly contacting with cationic Au, has been proposed in several mechanisms [50–52,57,59]. Up to now, however, no clear results and discussion about the number and locations of −OH species and their contribution on the stability of Au catalysts have been made.

For the spent parent Au/FLA catalyst in dry feed, HRTEM observations suggest a slight aggregation of gold nanoparticles with a change in mean diameter of gold particles from 1.59 nm before reaction to 1.85 nm after reaction. The similar results were observed with three kinds of spent 10% Fe/Au/FLA catalysts. The size increased from 4.05 to 4.37 nm when water was used as a solvent. This implies that the accumulation of carbonates-like species is the main reason for the catalyst deactivation in the study, which is in agreement with the results published in literature [5,12–17]. The smaller activity after thermal treatment on the spent parent Au/FLA catalyst might be ascribed to the incomplete removal of carbonates-like species because of quick reaction rate and direct deposition of the contaminates on the active sites.

For all spent modified catalysts, the fact that the activity can be totally recovered through in situ thermal treatment and better online stability over recovered catalysts (Fig. 9) is probably because the carbonates are preferably loaded on the out layer of iron oxides, not at the active sites. This matter suggests that indirect deposition of carbonates-like species on active sites (i.e., separating carbonates-like species from active sites) may assist in improving online stability of an Au catalyst. Large activity and stability over an Au@Fe_2O_3 core–shell structured catalyst was recently observed and reported by Yin et al. [41].

On the other hand, we noticed that the improvement in activity by water vapor for the Fe-modified catalyst (Fig. 12) was far smaller than that for the unmodified parent catalyst of Au/FLA.

This observation may mean that only those hydroxyl groups adjacent to Au nanoparticles can participate in the CO oxidation reaction: the reaction takes place at the Au-metal oxide interface, in consistent with the several reports [20,50,51,57].

5. Conclusions

Various amounts of iron oxides were post-added to a prepared Au catalyst via the wetness impregnation method with water, ethanol, or acetone as a solvent of iron precursor. The corresponding catalysts were investigated for their catalytic activities and online stabilities in the CO oxidation reaction process. The observations and results lead to the following conclusions:

- α-Fe_2O_3 was formed in the outmost layer of Fe-modified Au/FLA catalysts together with few Fe (II) species. The amounts of post-added Fe were observed similar in the catalysts as regard to the used solvents of water, ethanol, or acetone.
- Post-addition of Fe species leads to aggregation of nanogold particles with a gold particle size for the solvent used in the sequence of acetone <ethanol <water. The Fe-modified Au/FLA catalysts were found less active than the unmodified parent one with an activity sequence of the solvent opposite to the particle size of gold.
- Post-addition of Fe oxides can enhance the online stability of the Fe-modified Au catalysts. In situ thermal treatments can totally recover the spent modified catalysts with a better online stability regardless of the solvents used in the process of post-addition.
- Water as a solvent presented the best performance in the catalytic activity, online stability and activity recovery through in situ thermal treatment.
- The decreased activity of the Fe-modified catalyst can be significantly improved via modifying the preparation parameters.

Acknowledgements

References

[1] C.W. Corti, R.J. Holliday, Gold Bulletin 37 (2004) 20–26.
[2] C.W. Corti, R.J. Holliday, D.T. Thompson, Topics in Catalysis 44 (2007) 331–343.
[3] X. Xie, Y. Li, Z. Liu, M. Haruta, W. Shen, Nature 458 (2009) 746–749.
[4] M. Haruta, S. Tsubota, T. Kobayashi, H. Kageyama, M. Genet, B. Delmon, Journal of Catalysis 144 (1993) 175–192.
[5] M. Daté, M. Okumura, S. Tsubota, M. Haruta, Angewandte Chemie International Edition 43 (2004) 2129–2132.
[6] C. Qi, L. An, CatGold News, Gold Bulletin 41 (2008) CGN5–CGN5.
[7] D.T. Thompson, CatGold News, Gold Bulletin 40 (2007) C1–C2.
[8] L. An, S. Qi, X. Zou, WO Patent 007774 A1 (2006).
[9] R. Zanella, C. Louis, Catalysis Today 107–108 (2005) 768–777.
[10] X. Zou, S. Qi, Z. Suo, L. An, F. Li, Chinese Journal of Catalysis 27 (2006) 161–165.
[11] Y. Wu, K. Sun, J. Yu, B. Xu, Physical Chemistry Chemical Physics 10 (2008) 6399–6404.
[12] M. Azar, V. Caps, F. Morfin, J.L. Rousset, A. Piednoir, J.C. Bertolini, L. Piccolo, Journal of Catalysis 239 (2006) 307–312.
[13] J. Gong, C.B. Mullins, Journal of Physical Chemistry C 112 (2008) 17631–17634.
[14] Y. Denkwitz, B. Schumacher, G. Kučerová, R.J. Behm, Journal of Catalysis 267 (2009) 78–88.
[15] Y. Hao, M. Mihaylov, E. Ivanova, K. Hadjiivanov, H. Knozinger, B.C. Gates, Journal of Catalysis 261 (2009) 137–149.
[16] M. Raphulu, J. McPherson, G. Pattrick, T. Ntho, L. Mokoena, J. Moma, E. van der Lingen, Gold Bulletin 42 (2009) 328–336.
[17] C. Costello, M.C. Kung, H.S. Oh, Y. Wang, H.H. Kung, Applied Catalysis A 232 (2002) 159–168.
[18] F. Moreau, G.C. Bond, Topics in Catalysis 44 (2007) 95–101.
[19] F. Moreau, G.C. Bond, Catalysis Today 114 (2006) 362–368.

[20] M. Haruta, CATTECH 6 (2002) 102–115.
[21] M.S. Chen, D.W. Goodman, Science 306 (2004) 252–255.
[22] M. Chen, D.W. Goodman, Accounts of Chemical Research 39 (2006) 739–746.
[23] C. Xu, J. Su, X. Xu, P. Liu, H. Zhao, F. Tian, Y. Ding, Journal of the American Chemical Society 129 (2007) 42–43.
[24] M. Haruta, S. Tsubota, T. Kobayashi, H. Kageyama, M.J. Genet, B. Delmon, Journal of Catalysis 144 (1993) 175–192.
[25] G.C. Bond, D.T. Thompson, Gold Bulletin 33 (2000) 41–51.
[26] Z. Ma, C. Liang, S.H. Overbury, S. Dai, Journal of Catalysis 252 (2007) 119–126.
[27] X. Zhang, H. Wang, B. Xu, Journal of Physical Chemistry B 109 (2005) 9678–9683.
[28] M.A. Bollinger, M.A. Vannice, Applied Catalysis B 8 (1996) 417–443.
[29] J.A. Rodriguez, S. Ma, P. Liu, J. Hrbek, J. Evans, M. Pérez, Science 318 (2007) 1757–1760.
[30] M. Bandyopadhyay, O. Korsak, M.W.E. van den Berg, W.G. Birkner, W. Li, F. Schüth, H. Gies, Microporous and Mesoporous Materials 89 (2006) 158–163.
[31] P.M. Arnal, M. Comotti, F. Schuth, Angewandte Chemie International Edition 45 (2006) 8224–8227.
[32] K. Tanaka, Y. Morooka, K. Ishigure, T. Yajima, Y. Okabe, Y. Kato, H. Hamano, S. Sekiya, H. Tanaka, Y. Matsumoto, H. Koinuma, H. He, C. Zhang, Q. Feng, Catalysis Letters 92 (2004) 115–121.
[33] K. Tanaka, M. Shou, H. He, X. Shi, Catalysis Letters 110 (2006) 185–190.
[34] M. Shou, H. Takekawa, D. Ju, T. Hagiwara, D. Lu, K. Tanaki, Catalysis Letters 108 (2006) 119–124.
[35] A.A. Herzing, C.J. Kiely, A.F. Carley, P. Landon, G.H. Hutching, Science 321 (2008) 1331–1334.
[36] S.A. Sayari, A.F. Carley, S.H. Taylor, G.J. Hutchings, Topics in Catalysis 44 (2007) 123–128.
[37] M. Khoudiakov, M.C. Gupta, S. Deevi, Applied Catalysis A 291 (2005) 151–161.
[38] N.A. Hodge, C.J. Kiely, R. Whyman, M.R.H. Siddique, G.H. Hutchings, Q.A. Pankhurst, F.E. Wagner, R.R. Rajaram, S.E. Golunski, Catalysis Today 72 (2002) 133–144.
[39] G.Y. Wang, H.L. Lian, W.X. Zhang, D.Z. Jiang, T.H. Wu, Kinetics and Catalysis 43 (2002) 433–442.
[40] M.M. Schubert, S. Hackenberg, A.C. van Veen, M. Muhler, V. Plazak, R.J. Behm, Journal of Catalysis 197 (2001) 113–122.
[41] H. Yin, Z. Ma, M. Chi, S. Dai, Catalysis Today 160 (2011) 87–95.
[42] Q. Lin, L. An, J. Chen, H. Qin, S. Qi, X. Zou, Chinese Journal of Catalysis 29 (2008) 506–508.
[43] K. Fang, Microstructure Characterization of Micromaterials and Nanomaterials, Metallurgical Industry Press, Beijing, 2009 (in Chinese).
[44] P. Kumar, P. Sharma, R. Shrivastav, S. Dass, International Journal of Hydrogen Energy 36 (2011) 2777–2784.
[45] A.P. Grosvenor, B.A. Kobe, M.C. Biesinger, N.S. Mclntyre, Surface and Interface Analysis 36 (2004) 1564–1574.
[46] Z. Ma, S. Brown, S.H. Overbury, S. Dai, Applied Catalysis A 327 (2007) 226–237.
[47] W. Li, J. Fu, P. Gu, B. Yao, Z. Lin, Z. Zhou, Applied Catalysis B: Environmental 79 (2008) 402–409.
[48] W. Li, C. Massimiliano, S. Ferdi, Journal of Catalysis 237 (2006) 190–196.
[49] B. Schumacher, V. Plzak, M.J. Kinne, R. Behm, Catalysis Letters 89 (2003) 109–114.
[50] C.K. Costello, J.H. Yang, H.Y. Law, Y. Wang, J.N. Lin, L.D. Marks, M.C. Kung, H.H. Kung, Applied Catalysis A 243 (2003) 15–24.
[51] R.A. Ojifinni, N.S. Froemming, J. Gong, M. Pan, T.S. Kim, J.M. White, G. Henkelman, C.B. Mullins, Journal of the American Chemical Society 130 (2008) 6801–6812.
[52] K. Qian, W. Zhang, H. Sun, J. Fang, B. He, Y. Ma, Z. Jiang, S. Wei, J. Yang, W. Huang, Journal of Catalysis 277 (2011) 95–103.
[53] A.I. Kozlov, A.P. Kozlova, K. Asakura, Y. Matsui, T. Kogure, T. Shido, Y. Iwasawa, Journal of Catalysis 196 (2000) 56–65.
[54] R. Zanella, S. Giorgio, C.H. Shin, C.R. Henry, C. Louis, Journal of Catalysis 222 (2004) 357–367.
[55] Q. Fu, H. Saltsburg, M. Flytzani-Stephanopoulos, Science 301 (2003) 935–938.
[56] V. Schwartz, D.R. Mullins, W.F. Yan, B. Chen, S. Dai, S.H. Overbury, Journal of Physical Chemistry B 108 (2004) 15782–15790.
[57] M. Haruta, Faraday Discuss 152 (2011) 11–32.
[58] D. Wang, Z. Hao, D. Cheng, X. Shi, Journal of Chemical Technology and Biotechnology 81 (2006) 1246–1251.
[59] S.T. Daniells, A.R. Overweg, M. Makkee, J.A. Moulijn, Journal of Catalysis 230 (2005) 52–65.